

Supporting Information:

Molecular Parameters Governing the Elastic Properties of Brush Particle Films

Jaejun Lee ^a, Zongyu Wang ^b, Jianan Zhang ^{a,c}, Jiajun Yan ^{b#}, Tingwei Deng ^a, Yuqi Zhao ^a,
Krzysztof Matyjaszewski ^b, and Michael R. Bockstaller ^{a*}

^a Department of Materials Science and Engineering, Carnegie Mellon University, 5000 Forbes Ave., Pittsburgh, PA 15213, United States

^b Department of Chemistry, Carnegie Mellon University, 4400 Fifth Ave., Pittsburgh, Pennsylvania 15213, United States

^c School of Chemistry and Chemical Engineering, Anhui University, Hefei 230601, China

*) corresponding author: bockstaller@cmu.edu

#) current address: Lawrence Berkeley National Laboratory, Materials Sciences Division, One Cyclotron Road, Berkeley, CA 94720

Calculation of surface grafting density

Graft densities were calculated using the following equation:

$$\sigma_s = \frac{(1 - f_{\text{SiO}_2})N_A\rho_{\text{SiO}_2}d}{6f_{\text{SiO}_2}M_n} \quad (1)$$

The value for f_{SiO_2} , in the equation, is the weight fraction of silica measured by TGA after exclusion of any residual solvent; N_A is the Avogadro number; ρ_{SiO_2} is the density of silica NPs; d is the average diameter of silica NPs; M_n is the number average MW of polymer brushes.

Calculation of Poisson's ratio of composite materials

Poisson's ratio of brush particle materials were calculated using the Voigt model for composite materials¹:

$$\nu = \nu_{\text{org}}\phi_{\text{org}} + \nu_{\text{SiO}_2}\phi_{\text{SiO}_2} \quad (2)$$

where, ν_i is the Poisson's ratio of component i and ϕ_i is the volume fraction of component i .

Calculations were performed using $\nu_{\text{SiO}_2} = 0.17$, $\nu_{\text{PS}} = 0.34$, and $\nu_{\text{PMMA}} = 0.40$, respectively.

Table S1. Material information of (i-/d-) poly(methyl methacrylate) brush particles.

Sample ID	N	M_w/M_n	f_{org}	ϕ_{org}	σ_s (nm ⁻²)
SiO ₂ - <i>i</i> -MMA321*	321	1.20	0.81	0.89	0.44
SiO ₂ - <i>i</i> -MMA350*	359	1.15	0.82	0.90	0.42
SiO ₂ - <i>i</i> -MMA391*	391	1.23	0.85	0.91	0.46
SiO ₂ - <i>i</i> -MMA527*	527	1.21	0.87	0.93	0.43

Variables represent the degree of polymerization of graft, N ; dispersity index, M_w/M_n ; weight fraction of polymer, f_{org} ; volume fraction of polymer, ϕ_{org} ; surface grafting density, σ_s . Sample ID: SiO₂-(σ_s regime: d (dense) / i (intermediate) / s (sparse))-(monomer) N .

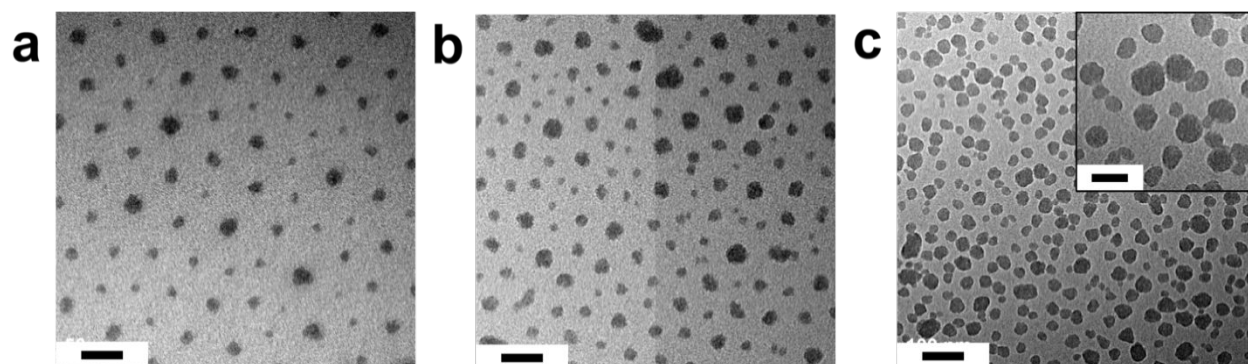


Figure S1. Representative bright field TEM for the (a) dense (SiO₂- d -MMA445), (b) intermediate (SiO₂- i -MMA563) and (c) sparse (SiO₂- s -MMA365) PMMA-brush systems with similar degrees of polymerization. All scale bars are 50 nm (20 nm in inset).

Quantitative analysis of domain structure using TEM micrographs

A quantitative analysis on TEM micrographs following a systematic processing was conducted using Matlab. A sequence for the analysis is shading correction – blurring – dilation – erosion – particle recognition – tessellation. Bandpass filter was applied to correct shading. As next steps, the combination of dilation and erosion was exploited to separate merged (neighboring) domains. Gaussian blurring is necessary to reduce detail for better recognition. Given that unstained TEM images provide 3 distinct contrast levels (dark (silica particles) and bright (polymer brush)), each domain was mapped by binarization. Then, particle domain was recognized, followed by Voronoi tessellation using centroid information. The results at each step are shown in Figure S2.

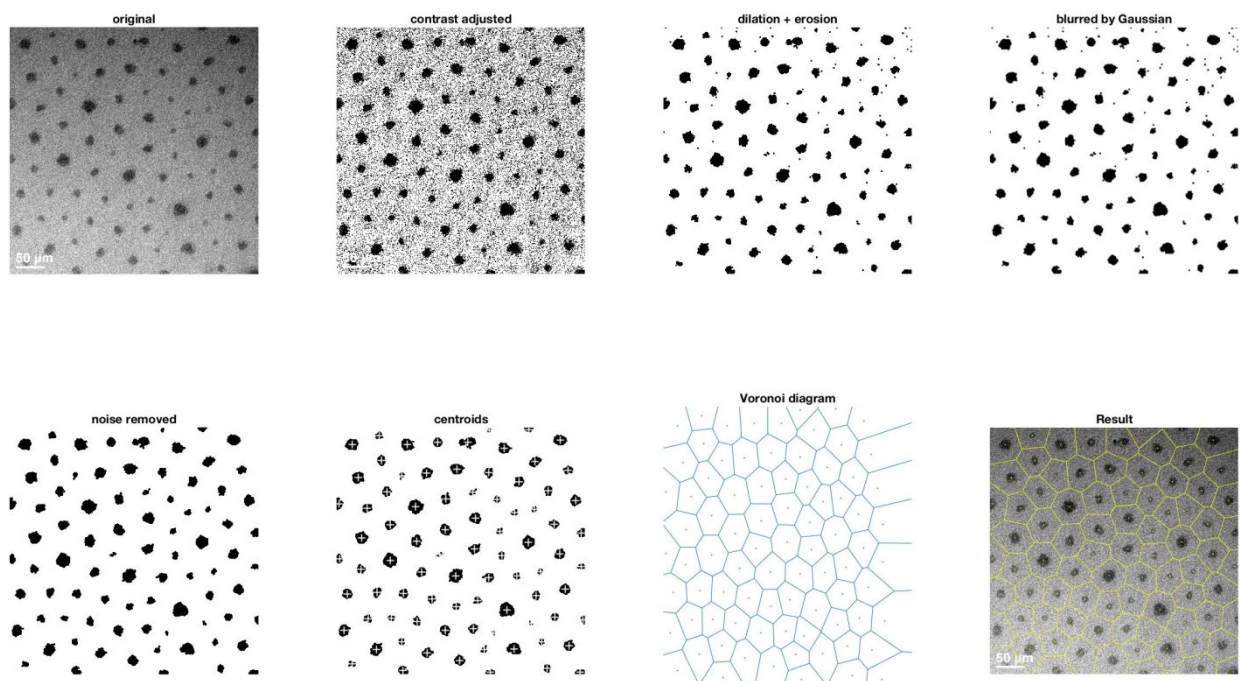


Figure S2. A representative image processing of a TEM micrograph (SiO_2 -*d*-MMA445) for Voronoi tessellation.

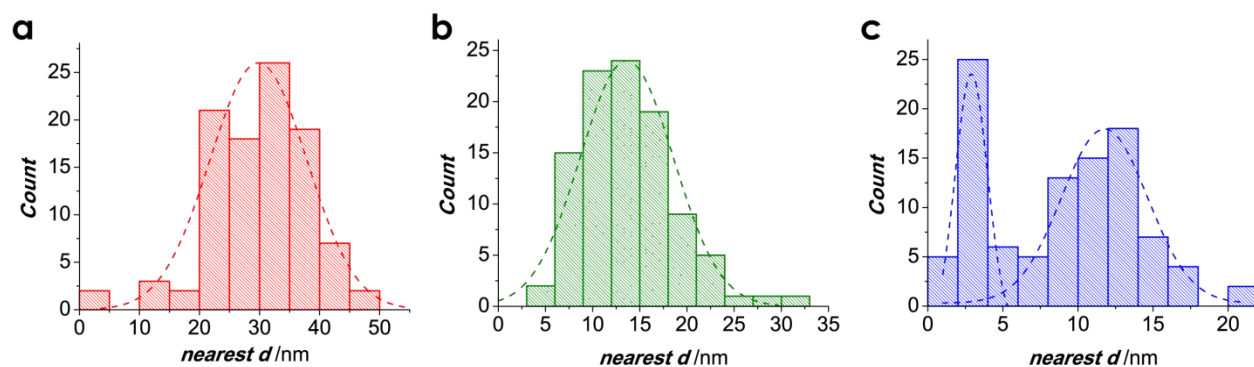


Figure S3. Histograms of spacing between adjacent particle cores in dense (a: SiO_2 -*d*-S365), intermediate (b: SiO_2 -*i*-S328) and sparse (c: SiO_2 -*s*-S432) systems. Monomodal distributions in the dense and intermediate materials indicate ‘isotropic’ microstructure while bimodal distribution in the sparse brush particles demonstrates ‘anisotropic’ structure.

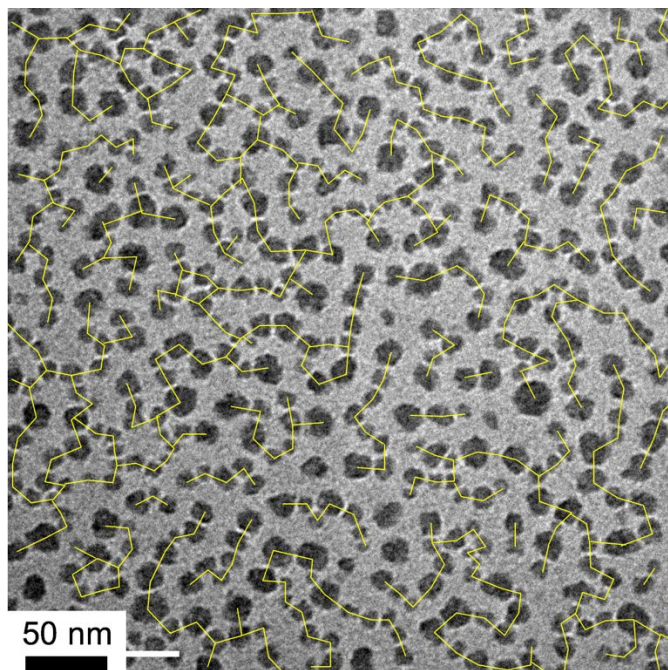


Figure S4. TEM image of SiO₂-s-S432 displaying string-like morphology. The number of particles per string was determined based on the analysis of next nearest neighbor distances as seen in the figure.

Identification of string-like morphologies in sparse brush particle materials (bulk state)

To differentiate the formation of string- vs. sheet-like superstructures in films of sparse brush particles, TEM imaging was performed on microsectioned bulk films. Due to the inherent brittleness of sparse brush materials, films were embedded into epoxy to enable sectioning. Figure S4 depicts a representative electron micrograph revealing the formation of string-like structures.

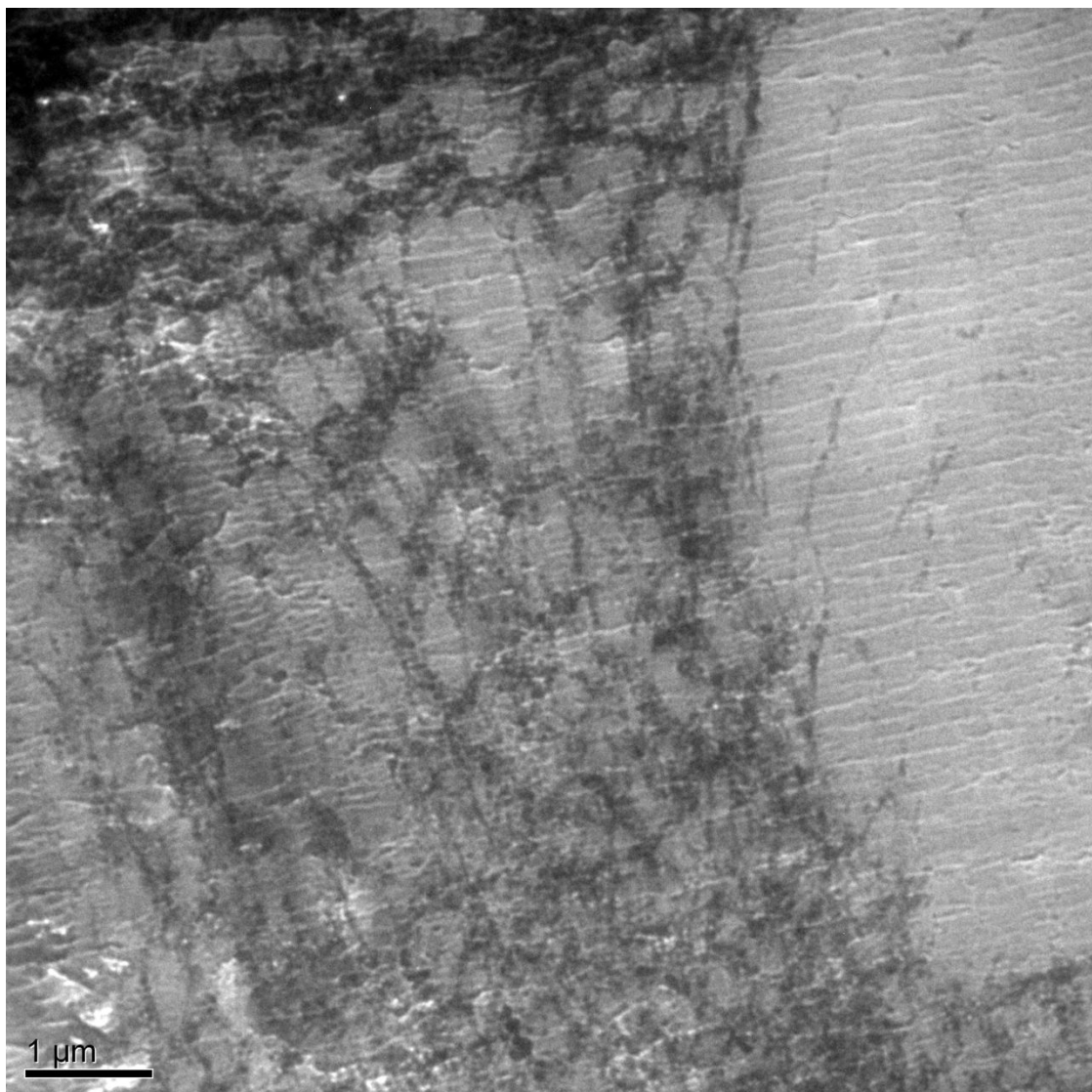
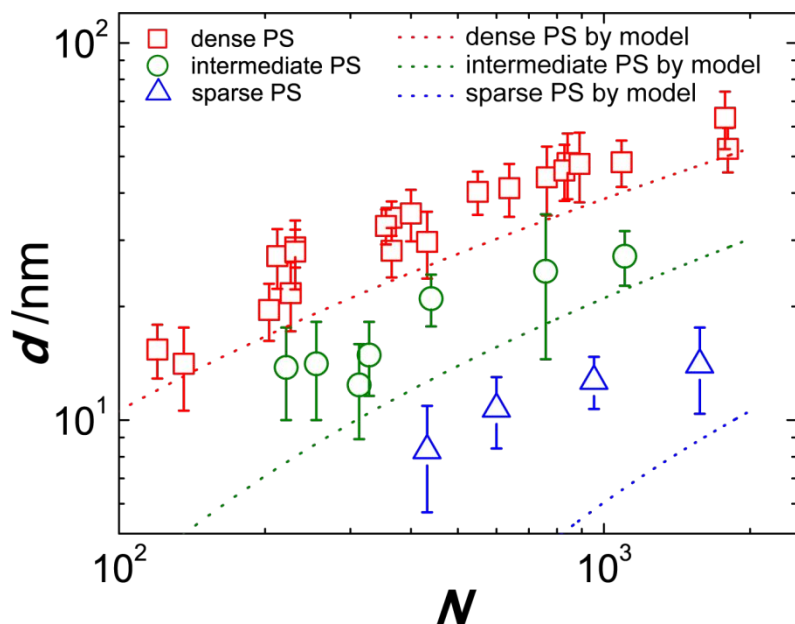


Figure S5. TEM micrograph revealing string-like particle superstructure in microsectioned film of SiO₂-s-S432.

Estimation of particle distance d based on inorganic volume fraction

To further support the conclusion of anisotropic superstructures in the case of sparse particle brush systems, the particle distance d was estimated based on the inorganic content using a procedure described by Glotzer et al (see text for more detail). The analysis reveals that the distances for dense and intermediate grafting density systems are reasonably well captured (small deviations occur because of the lateral expansion of chains in thin films). In contrast, the value for sparse systems is significantly under-estimated. This demonstrates the failure of the assumption of ‘uniform morphologies’ in the case of sparse brush particles.



Instrumented indentation analysis of brush particle films

Indentation experiments were performed as described in experimental section. Figure S6 displays representative load-displacement curves for brush particles films in the different grafting regimes. AFM analysis of indents was performed to rule out pile-up.

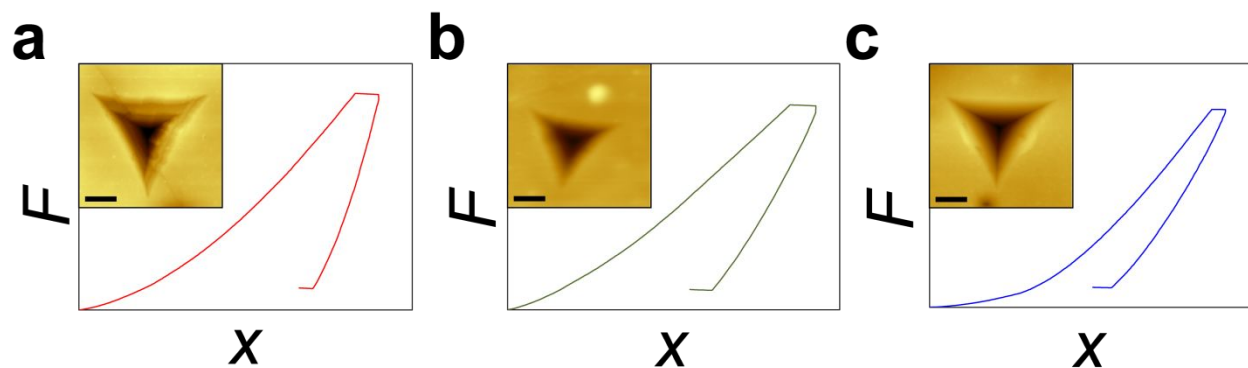


Figure S7. Representative load-displacement curves of (a) dense (SiO₂-d-S890), (b) intermediate (SiO₂-i-S328) and (c) sparse (SiO₂-s-S432) brush particulate films during nanoindentation measurements. Insets are corresponding topographs taken by AFM. All scale bars are 1 μm.

Comparison of cohesive energy contributed from core-core interaction and ligand-ligand interaction

A quantitative analysis of the effect of interpenetration between ligands is carried out. Herein we assume that there are only van der Waals interactions between nanoparticle cores, and London dispersion interactions between ligands. The model system we adopt for the estimation is silica nanoparticles ($r_0 = 7.9$ nm) grafted by PS chains. We also assumed the additivity of interactions to simplify the estimation.

First, the van der Waals interactions between two identical hard spheres² is:

$$U_c(d) = -\frac{A_{\text{SiO}_2}}{6} \left\{ \frac{2r_0^2}{(4r_0 + d)d} + \frac{2r_0^2}{(2r_0 + d)^2} + \ln \frac{(4r_0 + d)d}{(2r_0 + d)^2} \right\} \quad (2)$$

where, A_{SiO_2} is the Hamaker constant of silica in PS medium ($\sim 3.3 \times 10^{-21}$ J), r_0 is the radius of spherical particles, and d is the distance between particles. This cohesive energy is considerable when particles are very closely located. Otherwise, it is negligible.

The other interaction we consider is between overlapped (side-on) ligands. Dispersion interactions between end-on chains is insignificant as mentioned above. The interaction between two parallel ligands³ is:

$$U_l(L) = -C_{\text{PS}} \frac{3\pi L}{8\lambda^2 x^5} \quad (3)$$

where $C_{\text{PS}} \sim 7.1 \times 10^{-79}$ J·m⁶ is the interaction constant, L is the length of overlap between two parallel chains, λ is the contour length of the repeat unit (~ 0.252 nm), x is the intermolecular spacing between chains (~ 0.4 nm).⁴ We then extended the two interactions to our system. Assemblies of particle brush with relatively high grafting density have been known to form close packed structure in 2D⁵⁻¹⁰ and face-centered cubic (FCC) or hexagonal close packed (HCP) structure in 3D.⁸⁻¹⁰ Hence, each particle core is considered to neighbor with 12 cores at the closest distance with polymer buffer layer and forms a rhombic-dodecahedral unit cell. Similarly, each polymeric chain has 6 neighboring chains when closely packed. Under an assumption that densely grafted particles form a closed packed structure and are separated by a distance, d , the core-core interaction, U_{cc} , and the total ligand-ligand interaction, U_{ll} , per unit cell can be estimated as follows:

$$U_{cc}(d) = 12U_c(d) = -2A_{\text{SiO}_2} \left\{ \frac{2r_0^2}{(4r_0 + d)d} + \frac{2r_0^2}{(2r_0 + d)^2} + \ln \frac{(4r_0 + d)d}{(2r_0 + d)^2} \right\} \quad (4)$$

$$U_{ll}(d) = 6U_l(L) \frac{\lambda}{L} \rho_{st} V(d) = -6C_{\text{PS}} \frac{3\pi}{8\lambda x^5} \rho_{st} \left\{ \frac{\sqrt{2}}{2} (2r_0 + d)^3 - \frac{4}{3} \pi r_0^3 \right\} \quad (5)$$

As shown in Figure S7, U_{ll} is much stronger except for at extremely short separations (< 1 Å). For this reason, the core-core interaction is not considered when calculating an effective cohesive energy, U_{eff} , in particle brush assembly.

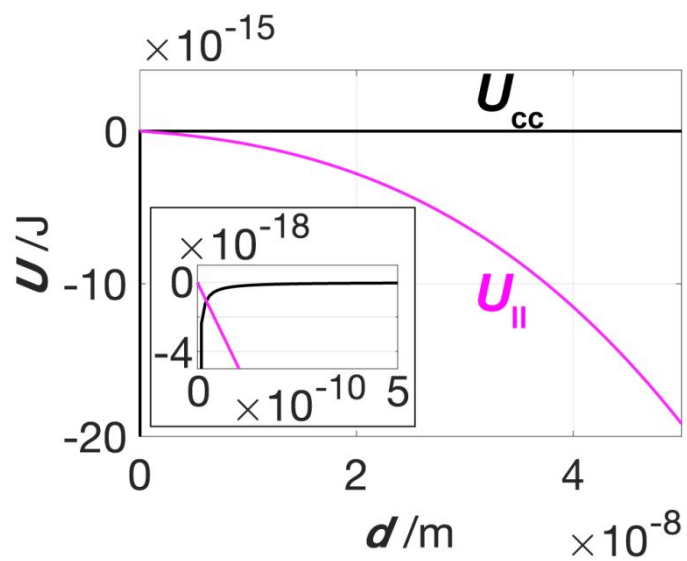


Figure S8. Comparison of interactions between inter-core, U_{cc} , and inter-ligand, U_{ll} . The inter-ligand dispersion interactions are dominant except for contact.

References (Supporting Information)

- (1) Ward, I. M.; Sweeney, J. *An Introduction to the Mechanical Properties of Solid Polymers*, 2nd ed.; Wiley, 2004.
- (2) Israelachvili, J. *Intermolecular and Surface Forces*, 3rd ed.; Academic Press, 2011. <https://doi.org/10.1016/C2009-0-21560-1>.
- (3) Salem, L. Attractive Forces between Long Saturated Chains at Short Distances. *J. Chem. Phys.* **1962**, *37* (9), 2100. <https://doi.org/10.1063/1.1733431>.
- (4) Gedde, U. W. *Polymer Physics*; Springer Science & Business Media, 1995. <https://doi.org/10.1007/978-94-011-0543-9>.
- (5) Hui, C. M.; Pietrasik, J.; Schmitt, M.; Mahoney, C.; Choi, J.; Bockstaller, M. R.; Matyjaszewski, K. Surface-Initiated Polymerization as an Enabling Tool for Multifunctional (Nano-)Engineered Hybrid Materials. *Chem. Mater.* **2014**, *26* (1), 745–762. <https://doi.org/10.1021/cm4023634>.
- (6) Choi, J.; Hui, C. M.; Pietrasik, J.; Dong, H.; Matyjaszewski, K.; Bockstaller, M. R.; Hui, M.; Pietrasik, J.; Dong, H.; Hui, C. M.; et al. Toughening Fragile Matter: Mechanical Properties of Particle Solids Assembled from Polymer-Grafted Hybrid Particles Synthesized by ATRP. *Soft Matter* **2012**, *8* (15), 4072. <https://doi.org/10.1039/c2sm06915f>.
- (7) Schmitt, M.; Choi, J.; Hui, C. M.; Chen, B.; Korkmaz, E.; Yan, J.; Margel, S.; Ozdoganlar, O. B.; Matyjaszewski, K.; Bockstaller, M. R. Processing Fragile Matter: Effect of Polymer Graft Modification on the Mechanical Properties and Processibility of (Nano-) Particulate Solids. *Soft Matter* **2016**, *12* (15), 3527–3537. <https://doi.org/10.1039/C6SM00095A>.
- (8) Goel, V.; Pietrasik, J.; Dong, H.; Sharma, J.; Matyjaszewski, K.; Krishnamoorti, R. Structure of Polymer Tethered Highly Grafted Nanoparticles. *Macromolecules* **2011**, *44* (20), 8129–8135. <https://doi.org/10.1021/ma200621r>.
- (9) Morinaga, T.; Ohno, K.; Tsujii, Y.; Fukuda, T. Structural Analysis of “Semisoft” Colloidal Crystals by Confocal Laser Scanning Microscopy. *Macromolecules* **2008**, *41* (10), 3620–3626. <https://doi.org/10.1021/ma7028665>.
- (10) Podsiadlo, P.; Krylova, G.; Lee, B.; Critchley, K.; Gosztola, D. J.; Talapin, D. V.; Ashby, P. D.; Shevchenko, E. V. The Role of Order, Nanocrystal Size, and Capping Ligands in the Collective Mechanical Response of Three-Dimensional Nanocrystal Solids. *J. Am. Chem. Soc.* **2010**, *132* (26), 8953–8960. <https://doi.org/10.1021/ja100464a>.